Supplementary Information for

Identifying climate model structural inconsistencies allows for tight constraint of aerosol radiative forcing

Leighton A. Regayre[1,2], Lucia Deaconu[3,4], Daniel P. Grosvenor[1,2,5], David M. H. Sexton[2], Christopher Symonds[5], Tom Langton[3], Duncan Watson-Paris[3], Jane P. Mulcahy[2], Kirsty J. Pringle[1,5,6], Mark Richardson[5], Jill S. Johnson[1,7], John W. Rostron[2], Hamish Gordon[1,8], Grenville Lister[9,10], Philip Stier[3] and Ken S. Carslaw[1]

[1]Institute for Climate and Atmospheric Science, School of Earth and Environment, University of Leeds, Leeds, LS2 9JT, UK
[2]Met Office Hadley Centre, Exeter, Fitzroy Road, Exeter, Devon, EX1 3PB, UK
[3]Atmospheric, Oceanic and Planetary Physics Department, University of Oxford, Oxford, OX1 3PU
[4]Faculty of Environmental Science and Engineering, Babes-Bolyai University, Cluj, Romania, 400294
[5]Centre for Environmental Modelling and Computation, School of Earth and Environment, University of Leeds, Leeds, LS2 9JT, UK
[6]Edinburgh Parallel Computing Centre, Bayes Centre, University of Edinburgh, EH8 9BT
[7]School of Mathematics and Statistics, University of Sheffield, Sheffield, S3 7RH, UK
[8]Department of Chemical Engineering and Center for Atmospheric Particle Studies, Carnegie Mellon University, Pittsburgh, PA 15213,USA
[9]Department of Meteorology, University of Reading, RG6 6AH, UK
[10]National Centre for Atmospheric Science, Reading, RG6 6AH, UK

Leighton Regayre
Email: L.A.Regayre@leeds.ac.uk

This PDF file includes:

Figures S1 to S29
Tables S1 to S4

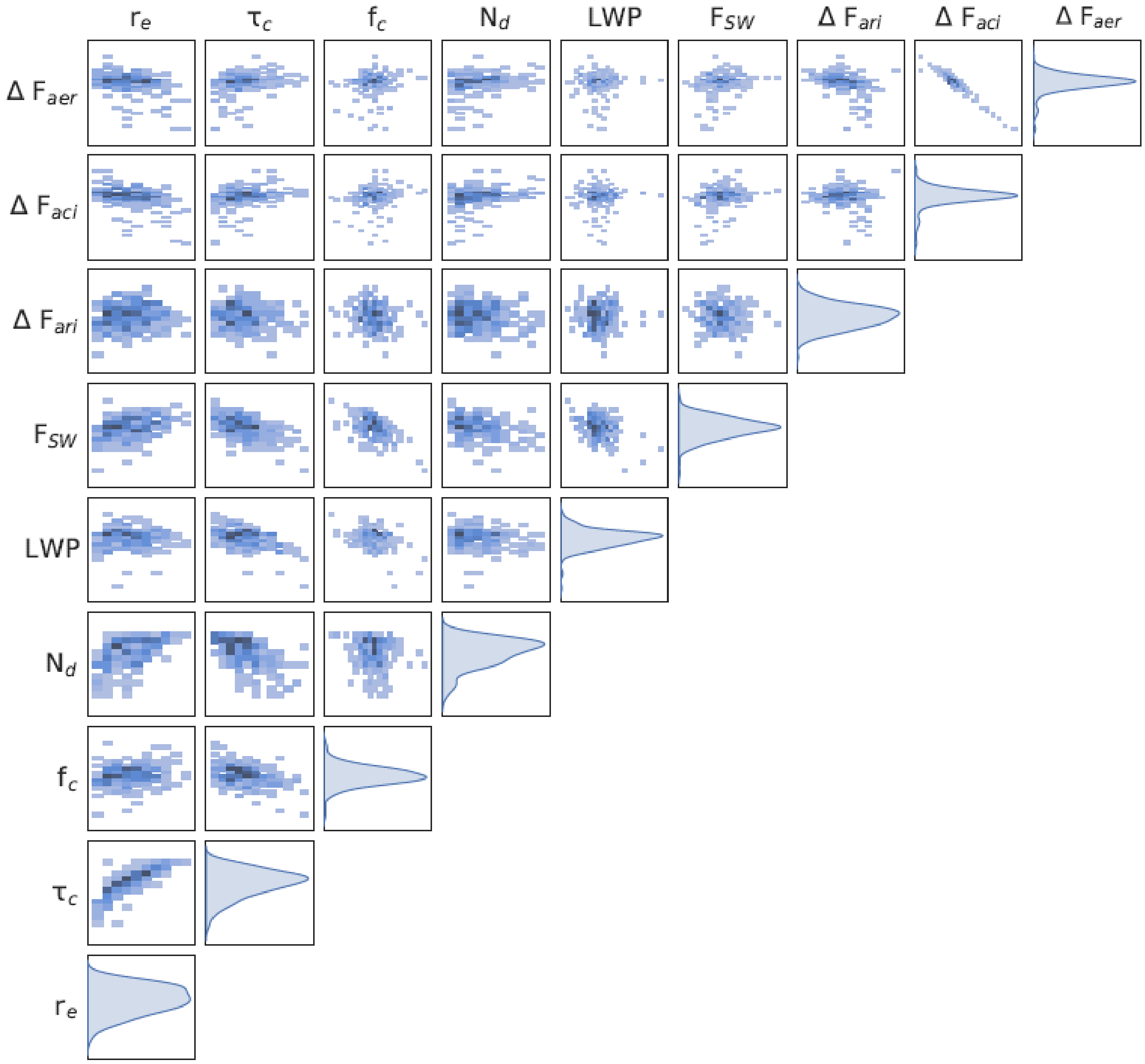

Fig. S1: Density plots of global, annual mean output from 221 PPE members for ΔF_{aer}, ΔF_{aci}, ΔF_{ari}, and global mean F_{SW}, LWP, N_d, f_c,τ_c and r_e,. Diagonal panels show probability density functions for individual variables.

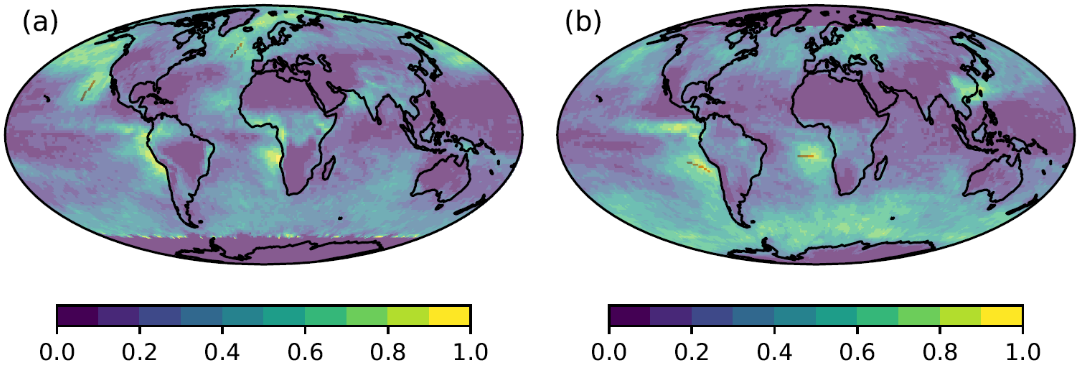

Fig. S2: **Transects from stratocumulus to cumulus cloud dominated regions in a) July and b) November, superimposed on MODIS liquid cloud fraction values for the corresponding month.**

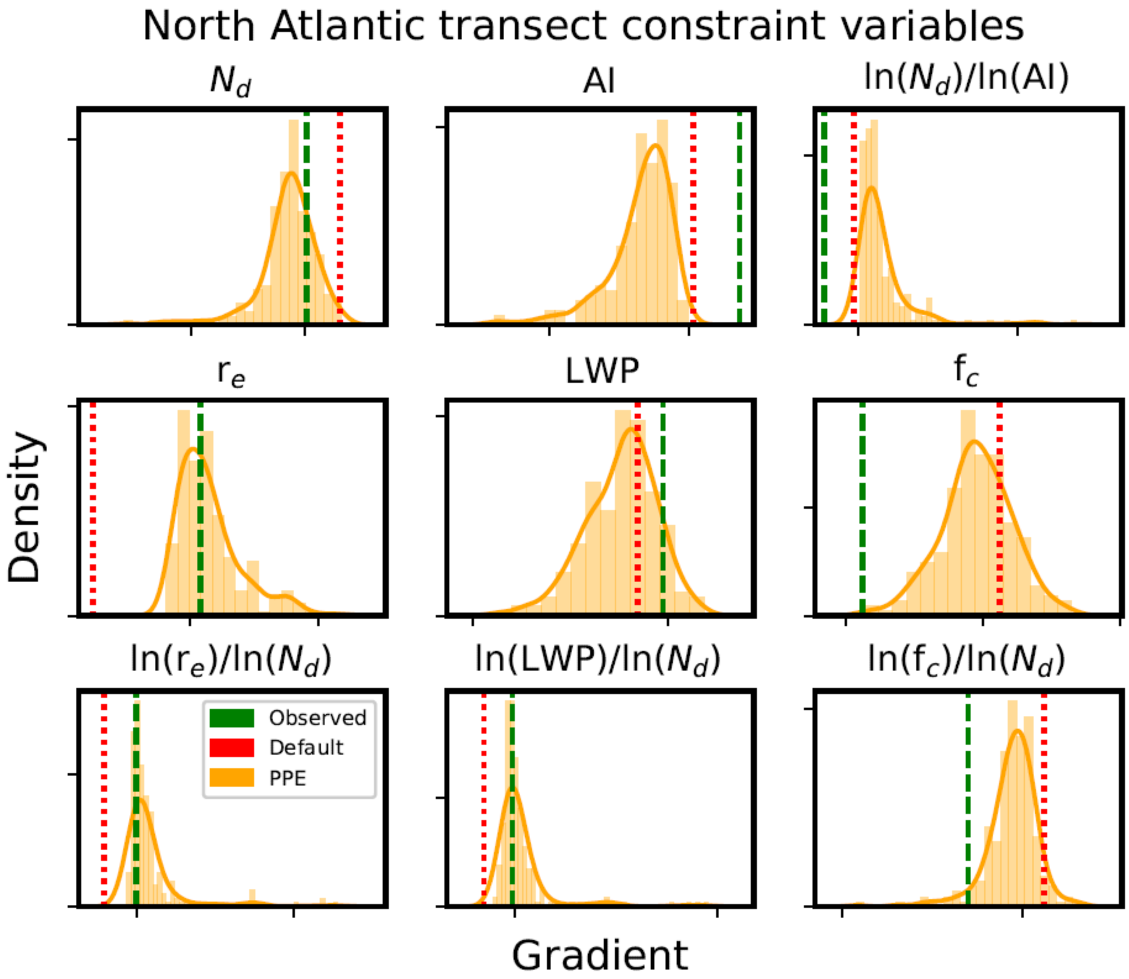

Fig. S3: Probability density functions of North Atlantic transect constraint variables.

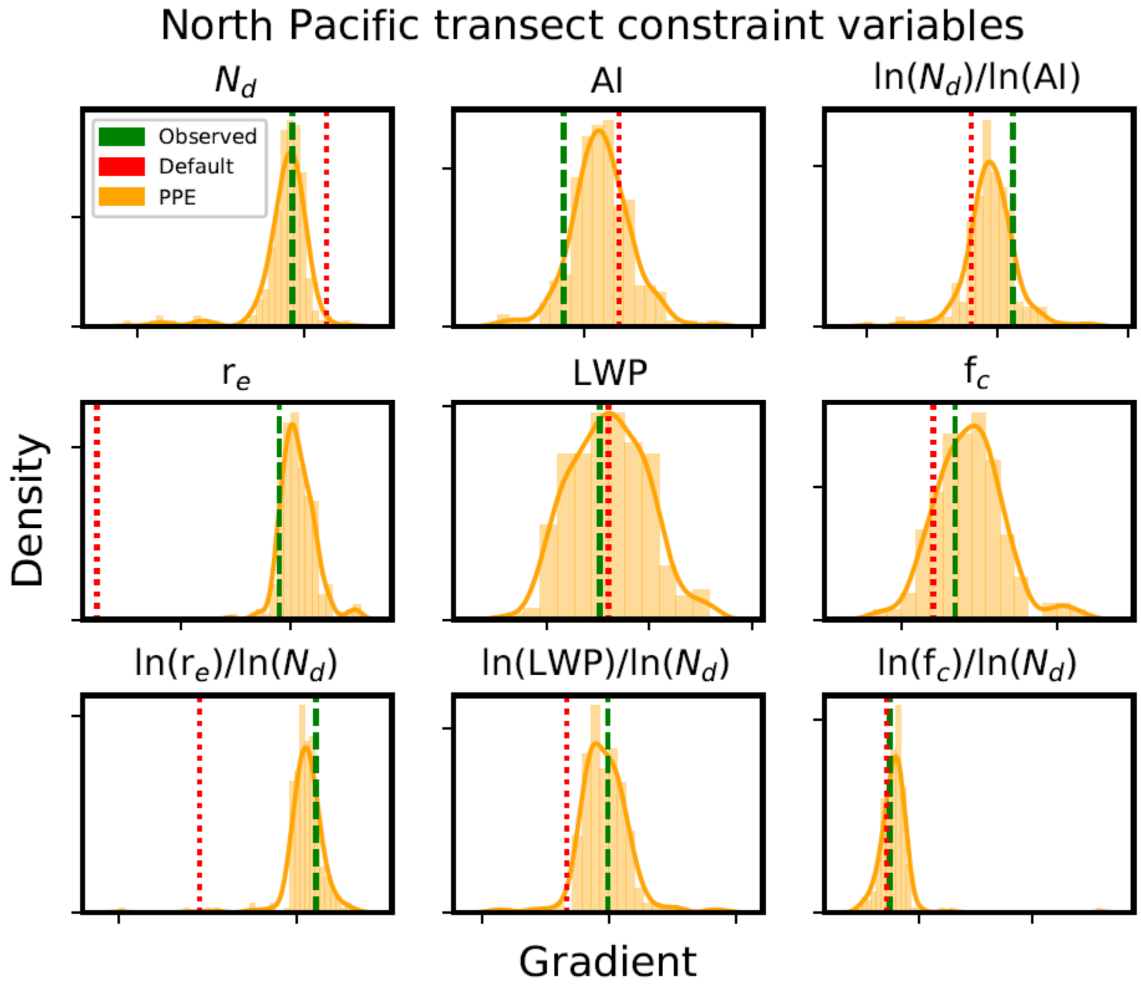

Fig. S4: Probability density functions of North Pacific transect constraint variables.

55

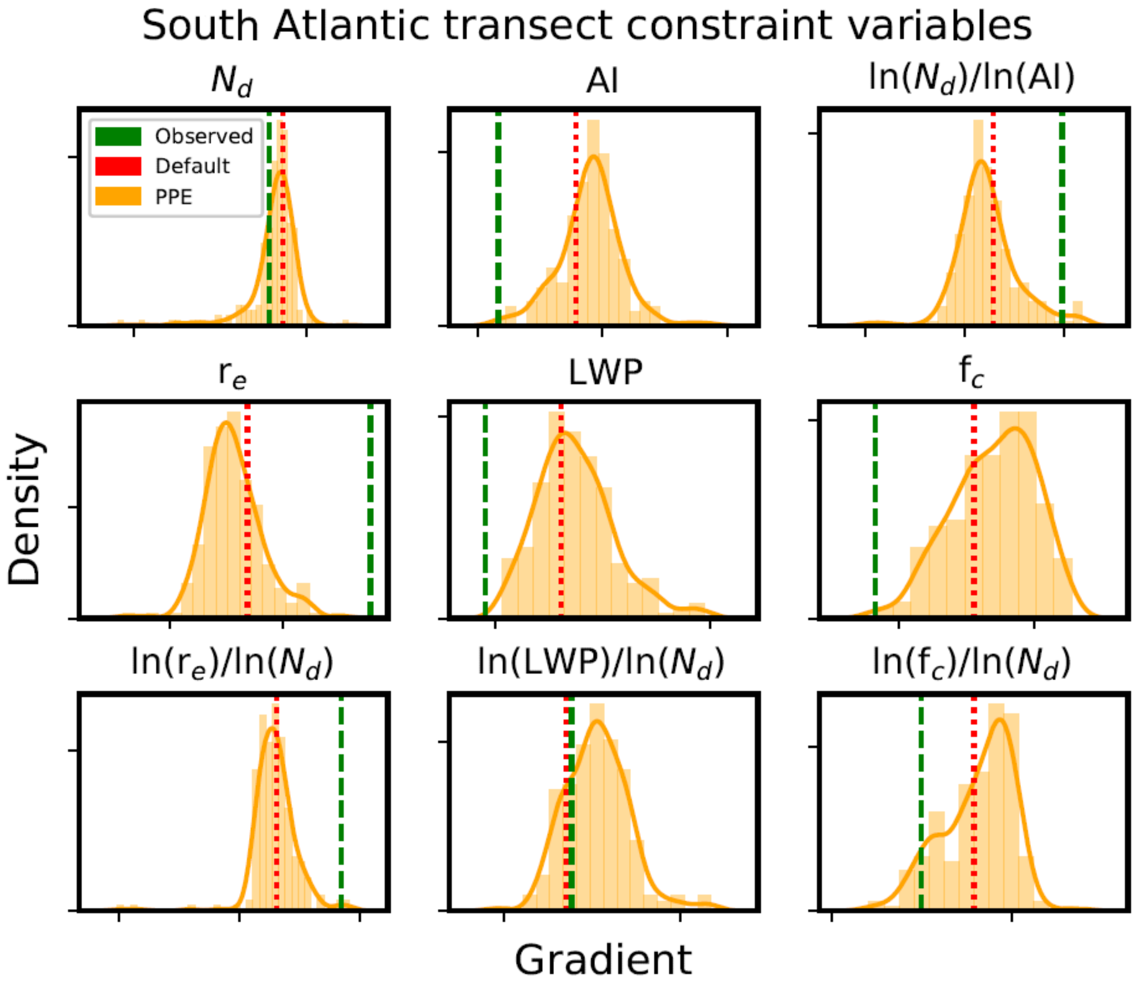

Fig. S5: Probability density functions of South Atlantic transect constraint variables.

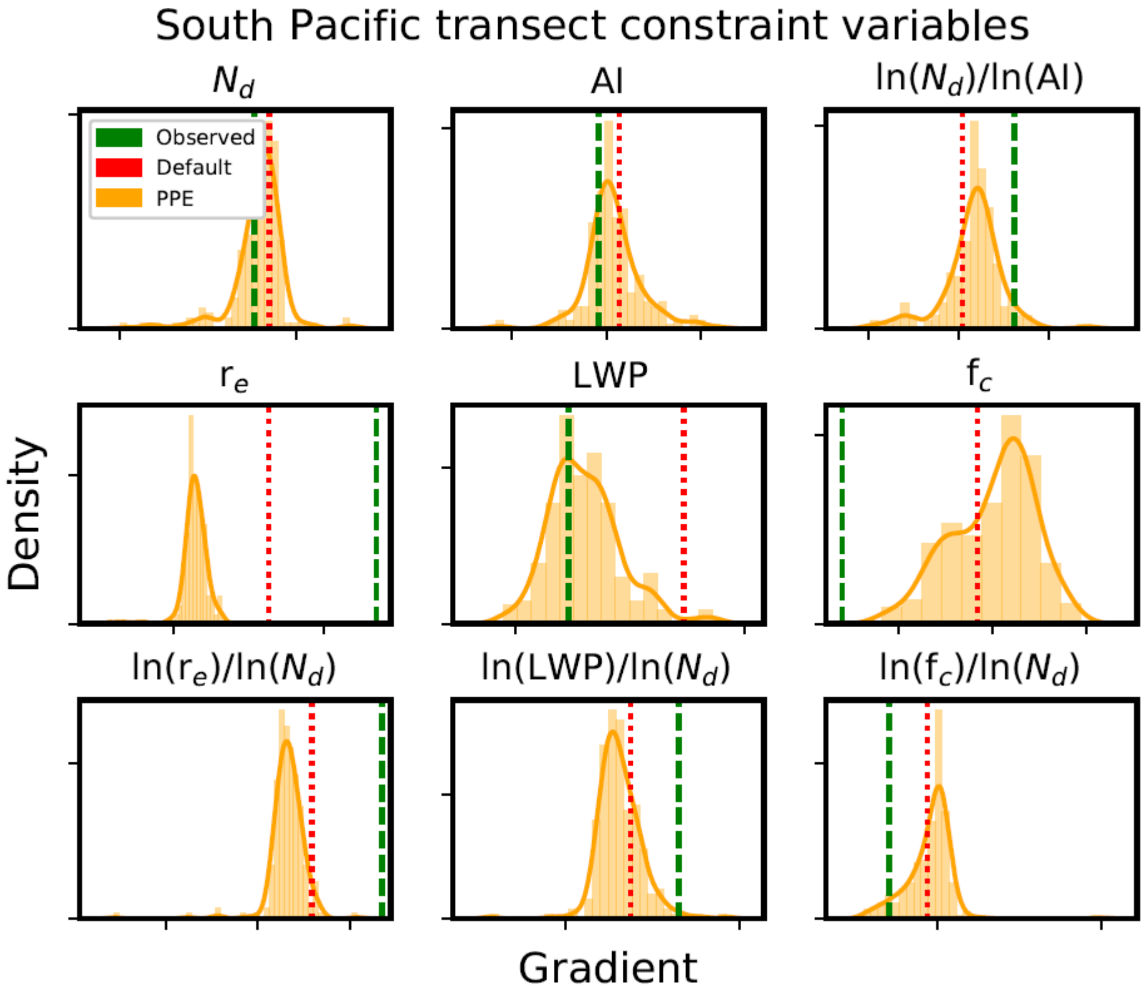

60 **Fig. S6: Probability density functions of South Pacific transect constraint variables.**

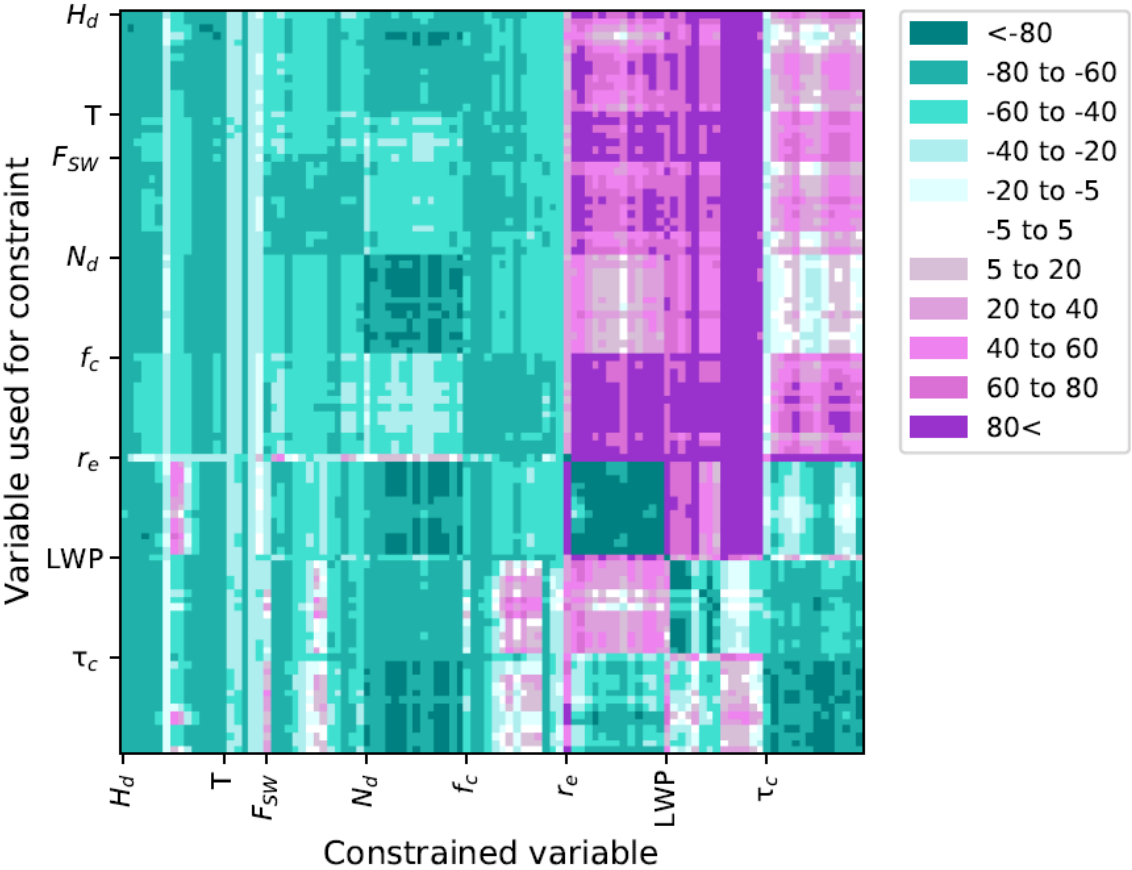

Fig. S7: Pairwise comparisons of North Pacific and H_d constraint variables. Figure features are identical with Fig. 5.

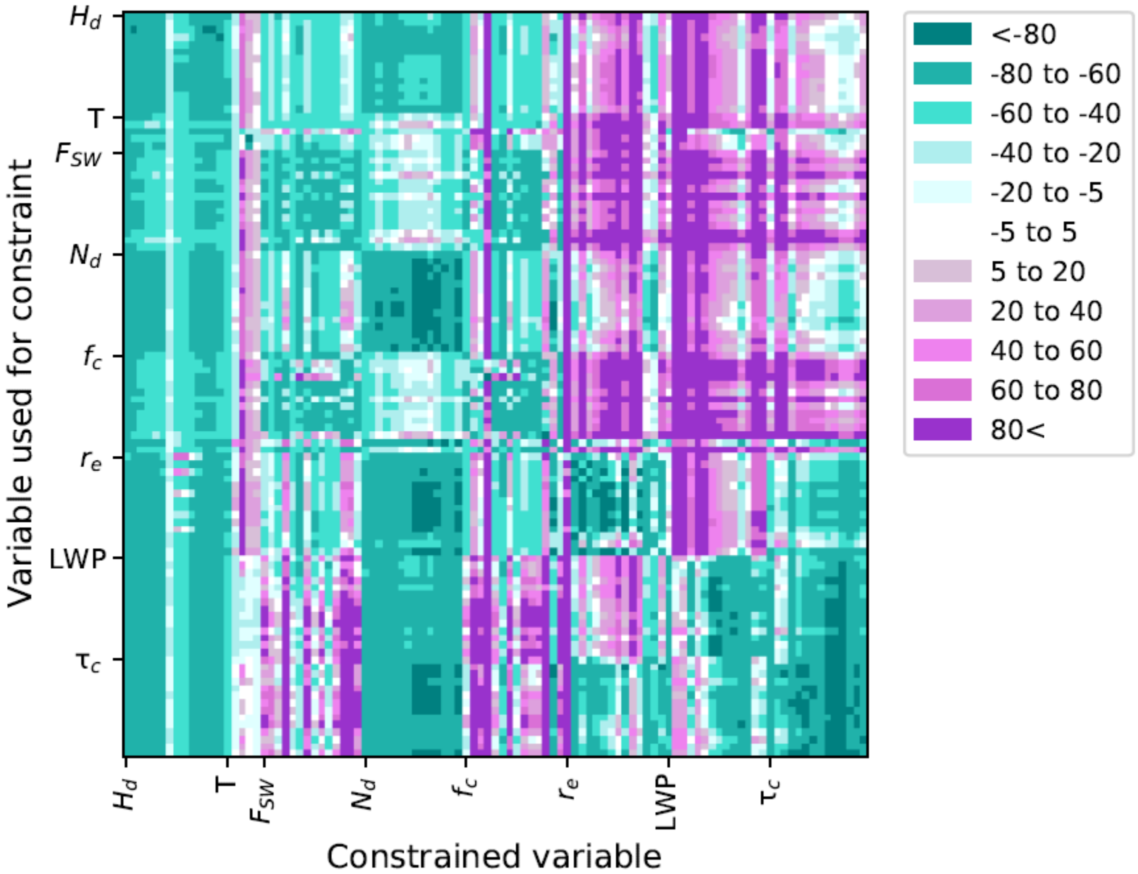

Fig. S8: Pairwise comparisons of South Atlantic and H_d constraint variables. Figure features are identical with Fig. 5.

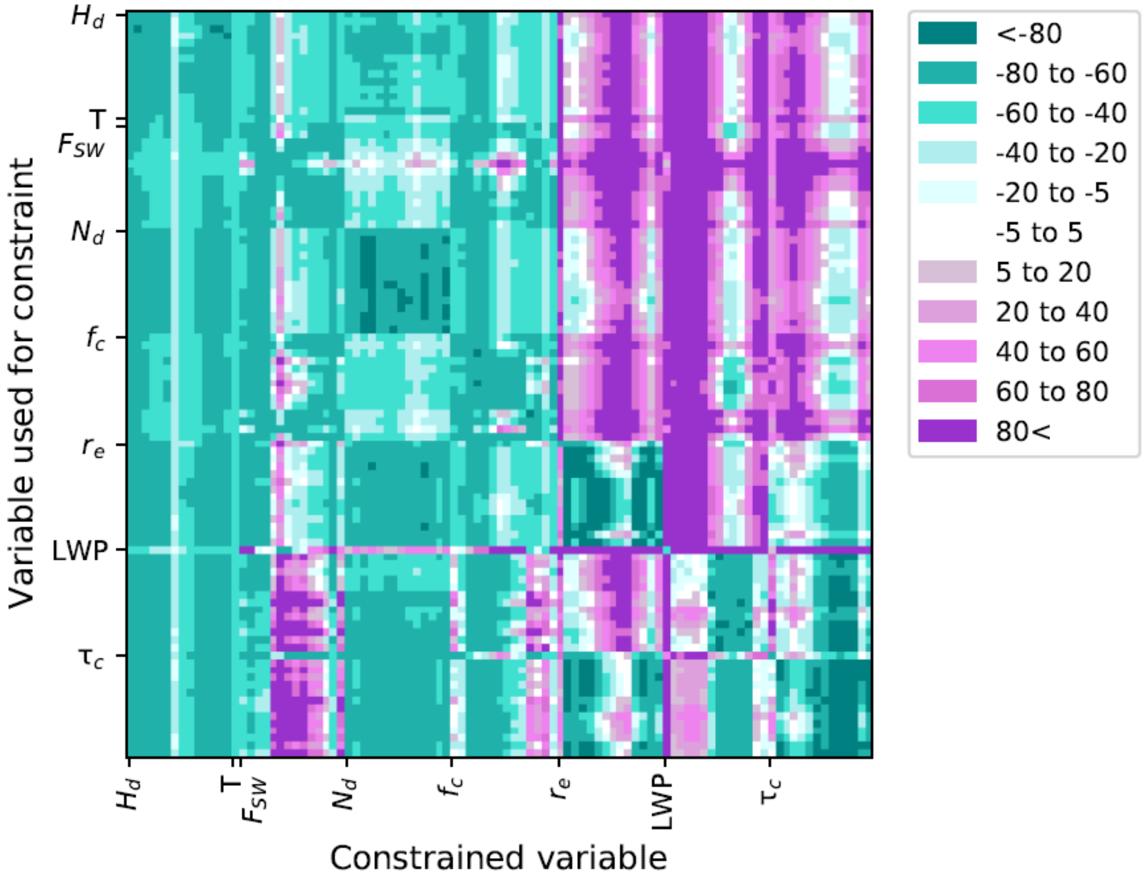

Fig. S9: Pairwise comparisons of South Pacific and H_d constraint variables. Figure features are identical with Fig. 5.

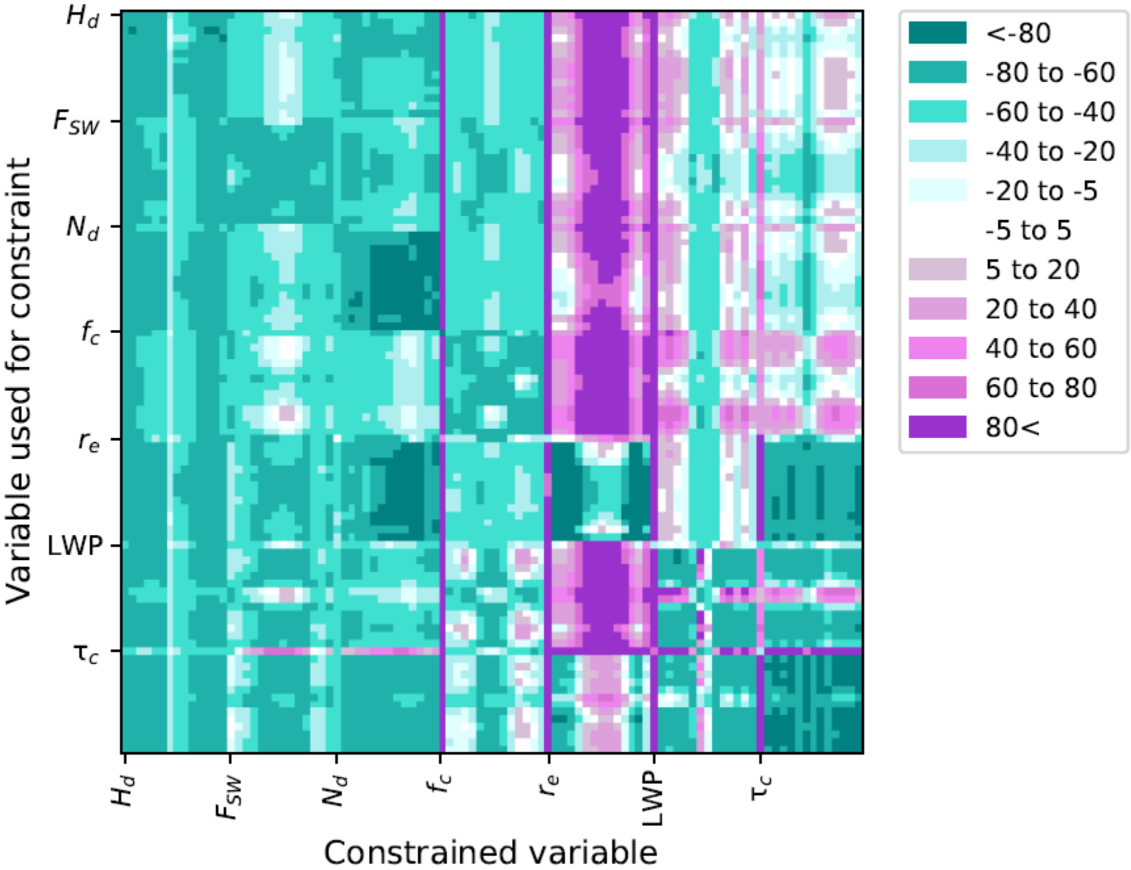

Fig. S10: Pairwise comparisons of Southern Ocean and H_d constraint variables. Figure features are identical with Fig. 5. 80

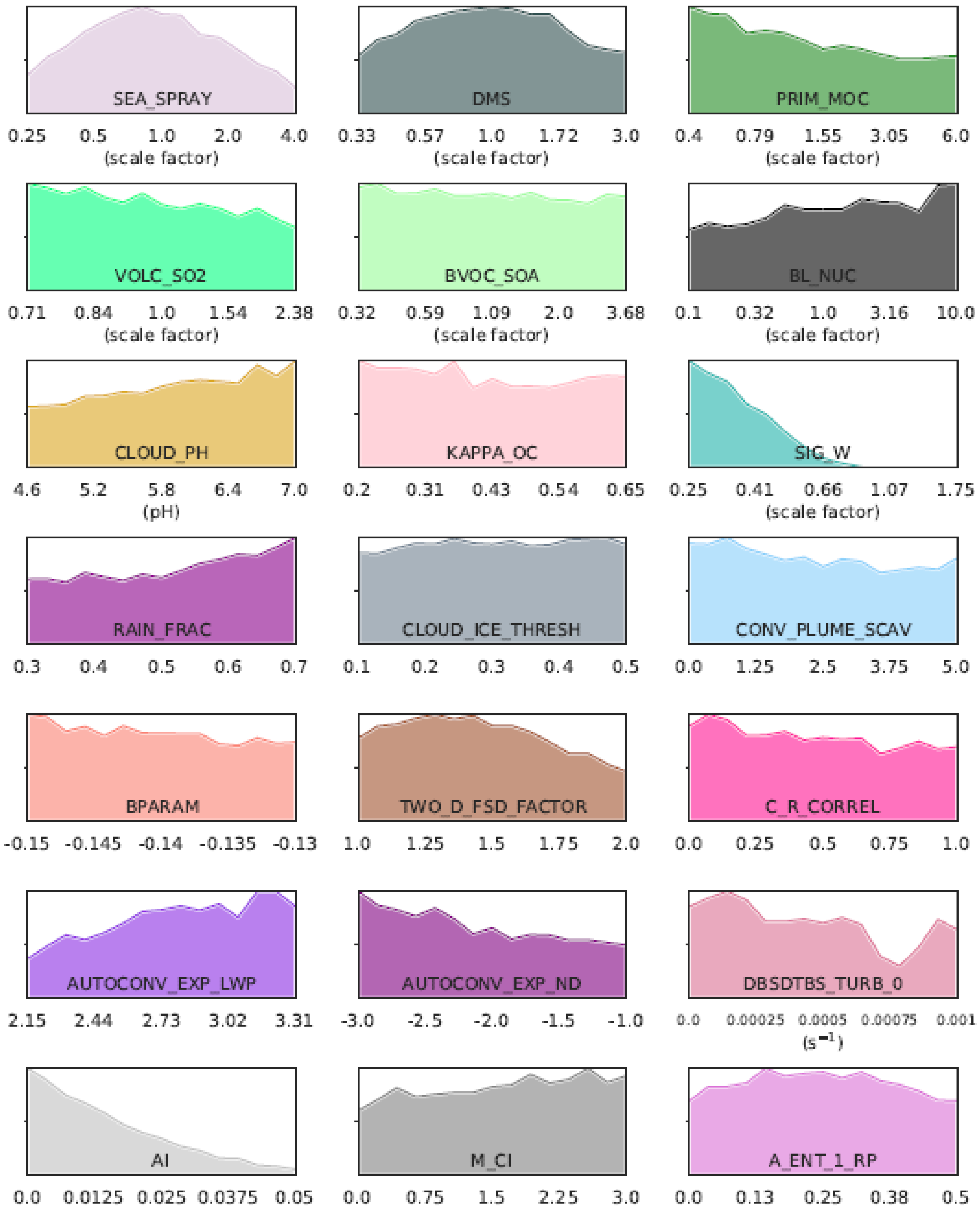

Fig. S11: Probability density functions of model parameters after constraint using our optimal set of constraint variables. In the original sample of 1 million model variants, these pdfs would be uniformly distributed on this scale. Non-shaded sections indicate a proportion of model variants with corresponding parameter values have been ruled out as implausible.

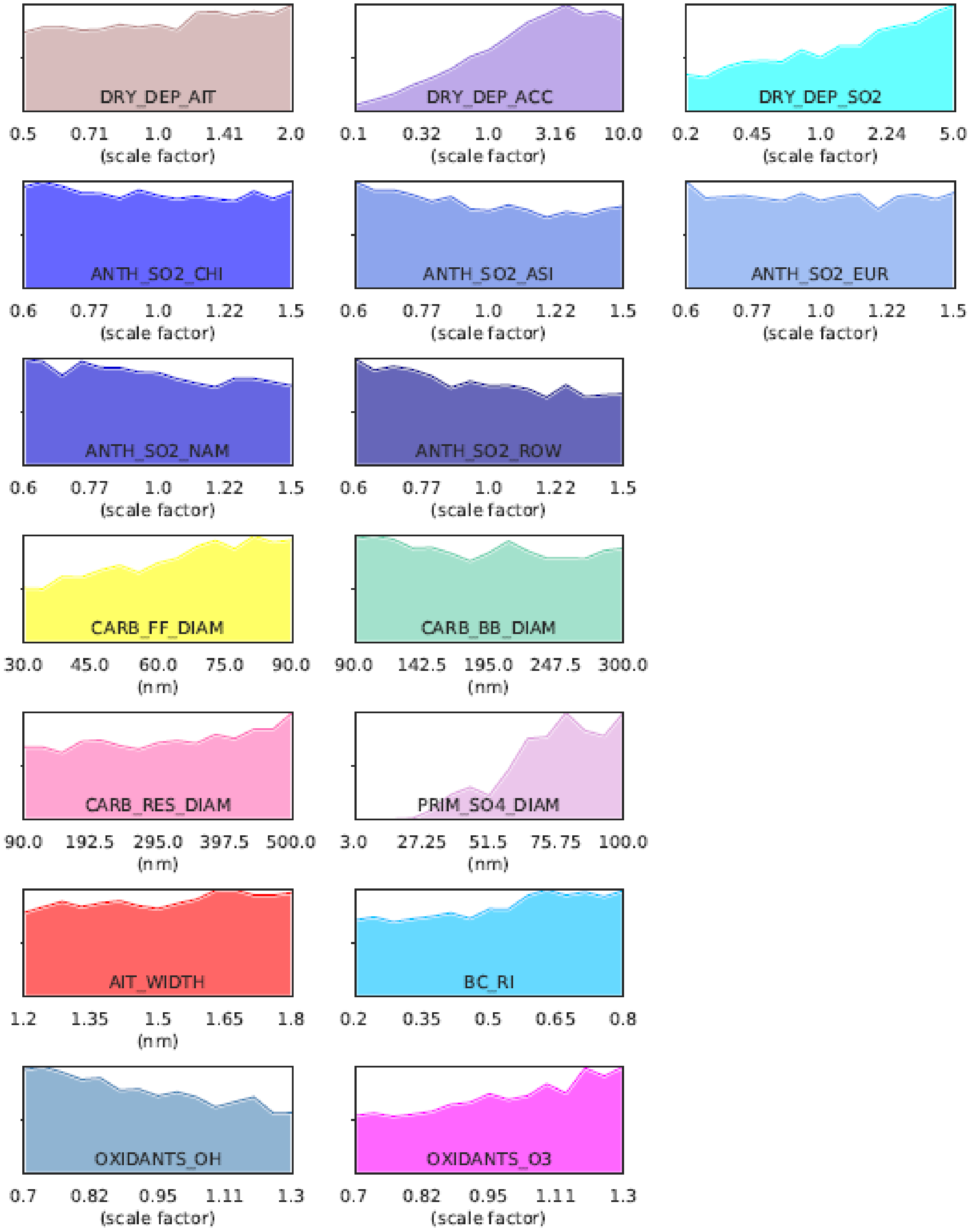

Fig. S12: Probability density functions of model parameters after constraint using our optimal set of constraint variables. Features are identical to Fig. S11.

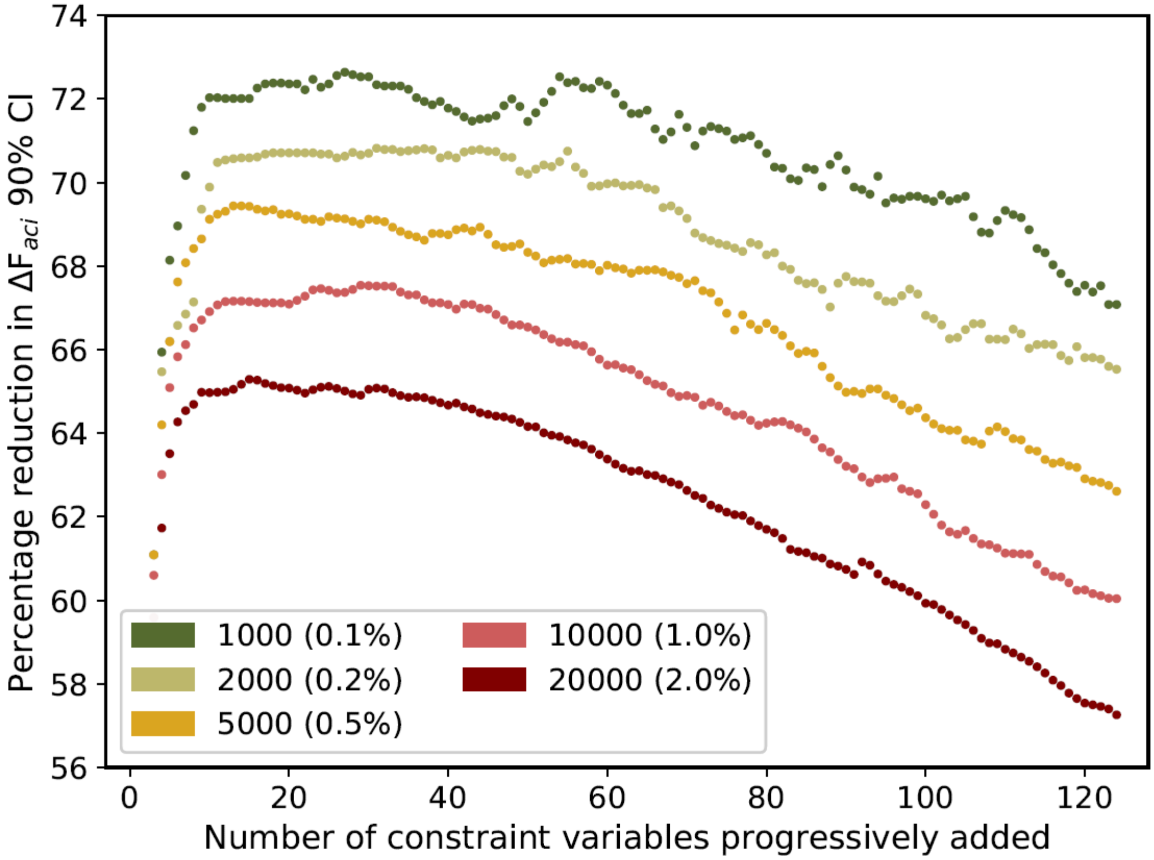

Fig. S13: Constraint of ΔF_{aci} and the effect of varying the number of constraint variables used and the number of model variants retained (percentage of original 1 million) at each stage of the constraint (legend). The constraints achieved by retaining 5000 model variants at each stage is identical to the constraints shown in Fig. 6.

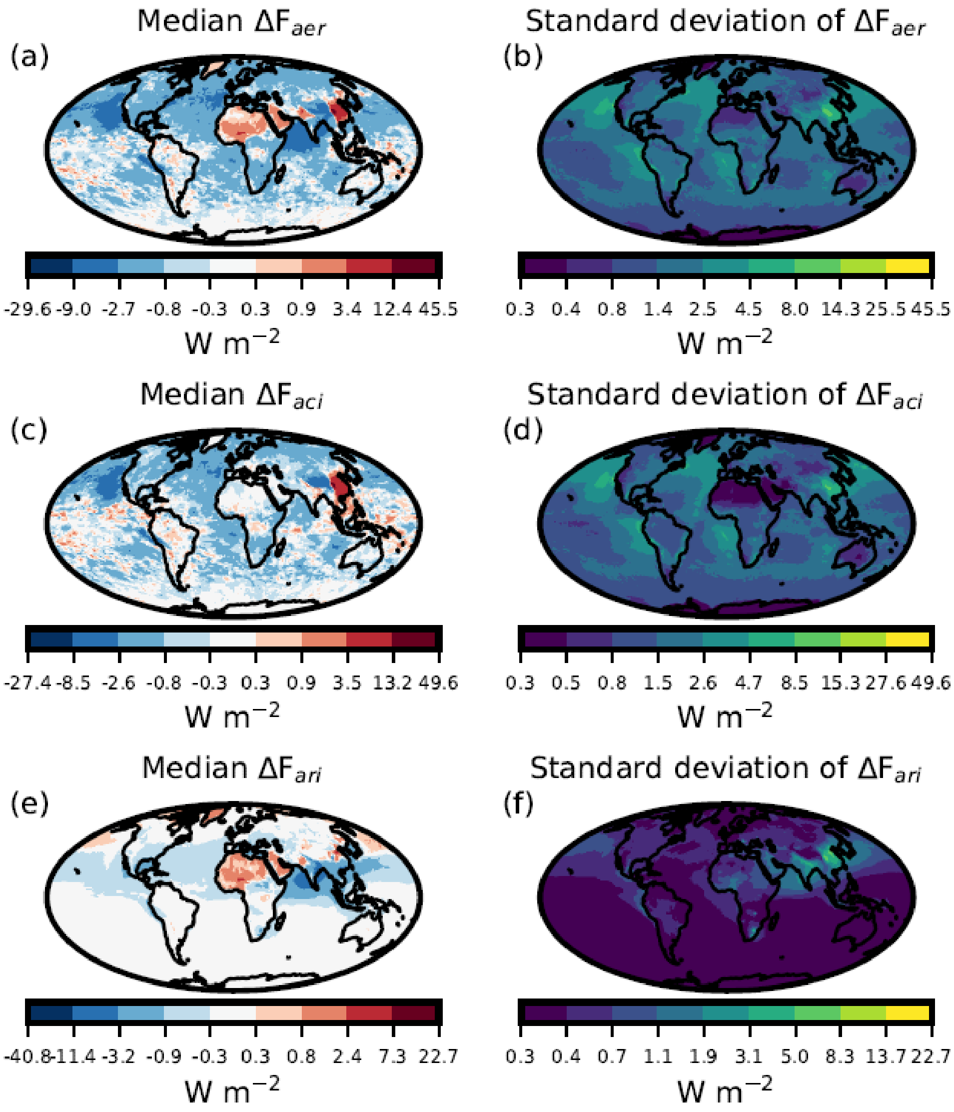

100 **Fig. S14: Median and standard deviations of annual mean Δ*F*$_{aer}$, Δ*F*$_{aci}$ and Δ*F*$_{ari}$, across the 221 PPE members. Values were calculated in each model grid box independently.**

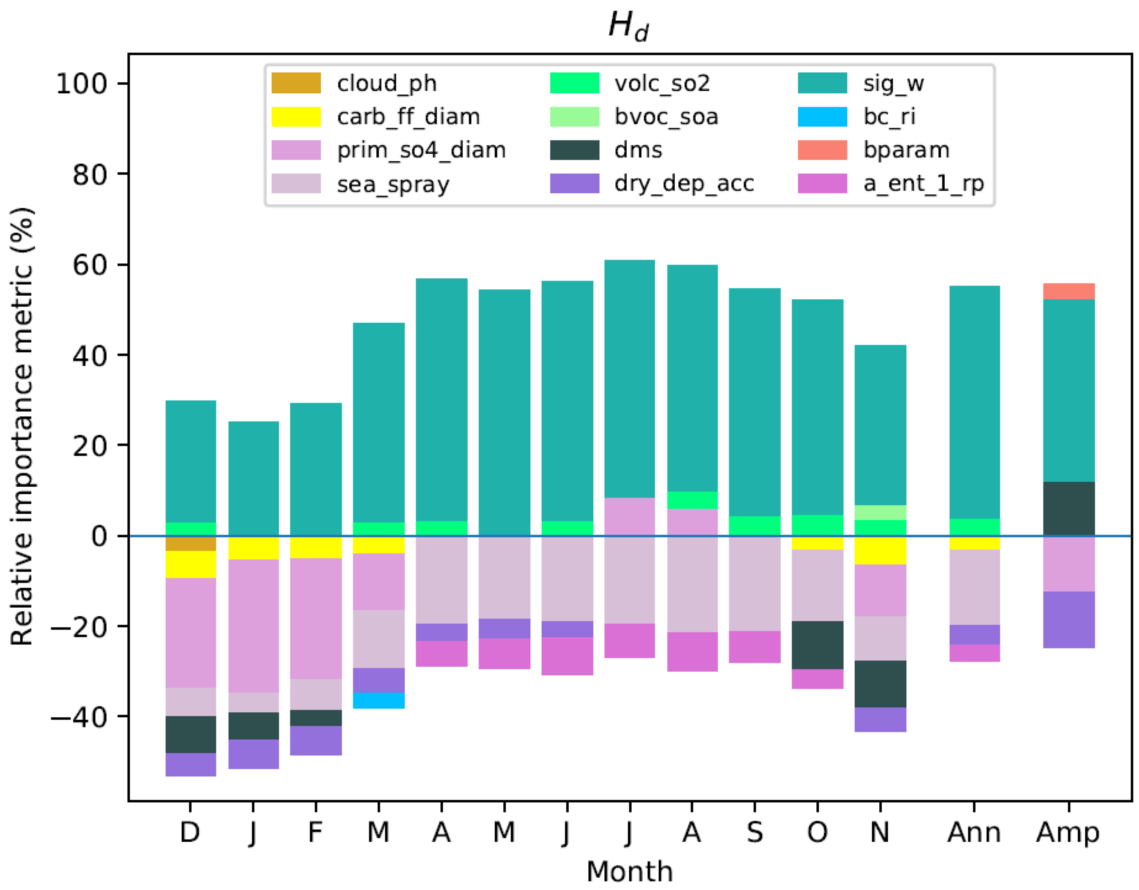

Fig. S15: Relative importance of model parameters as causes of uncertainty in H_d. Relative importance metrics are calculated for each month (December 2016 to November 2017), for the annual mean (Ann) and the seasonal amplitude (Amp). Relative importance metrics lower than 4% are not shown.

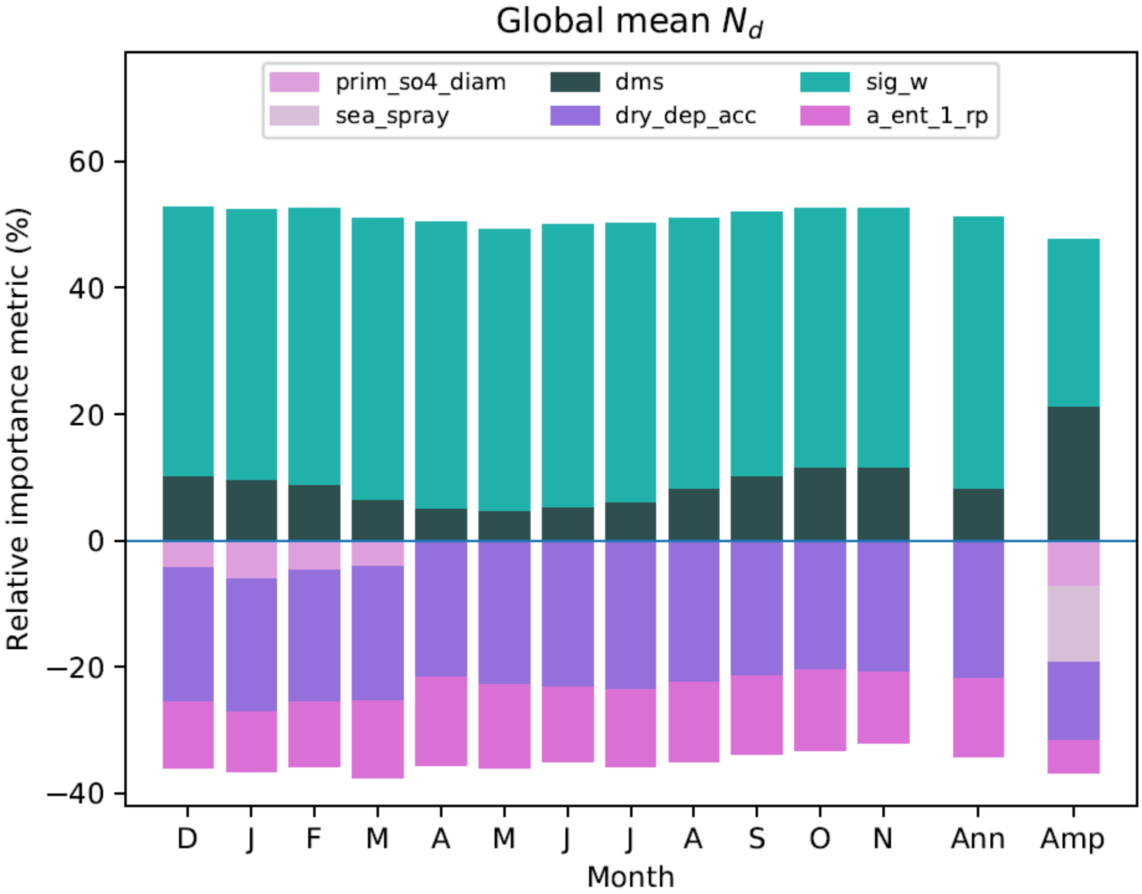

Fig. S16: Relative importance of model parameters as causes of uncertainty in global mean N_d. Figure features are identical to Fig. S15.

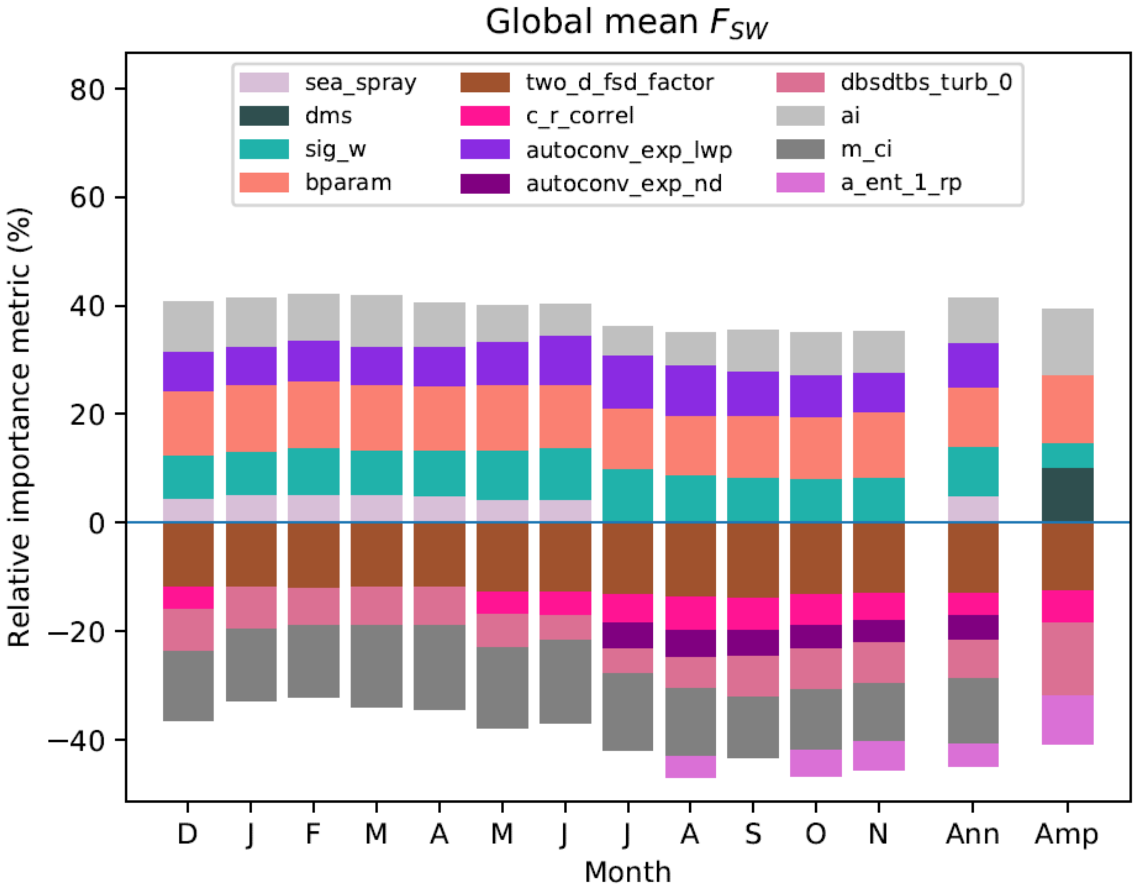

Fig. S17: Relative importance of model parameters as causes of uncertainty in global mean
115 **F_{SW}. Figure features are identical to Fig. S15.**

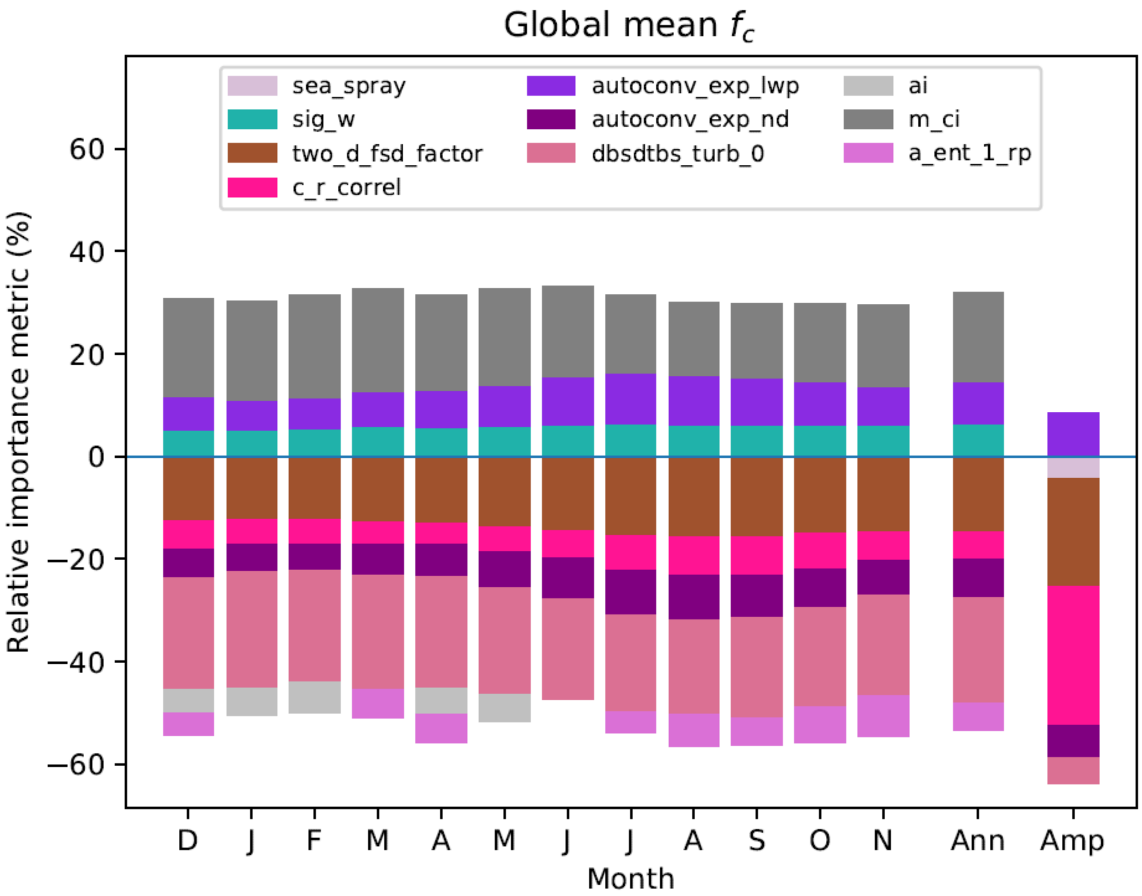

Fig. S18: Relative importance of model parameters as causes of uncertainty in global mean f_c. Figure features are identical to Fig. S15.

120

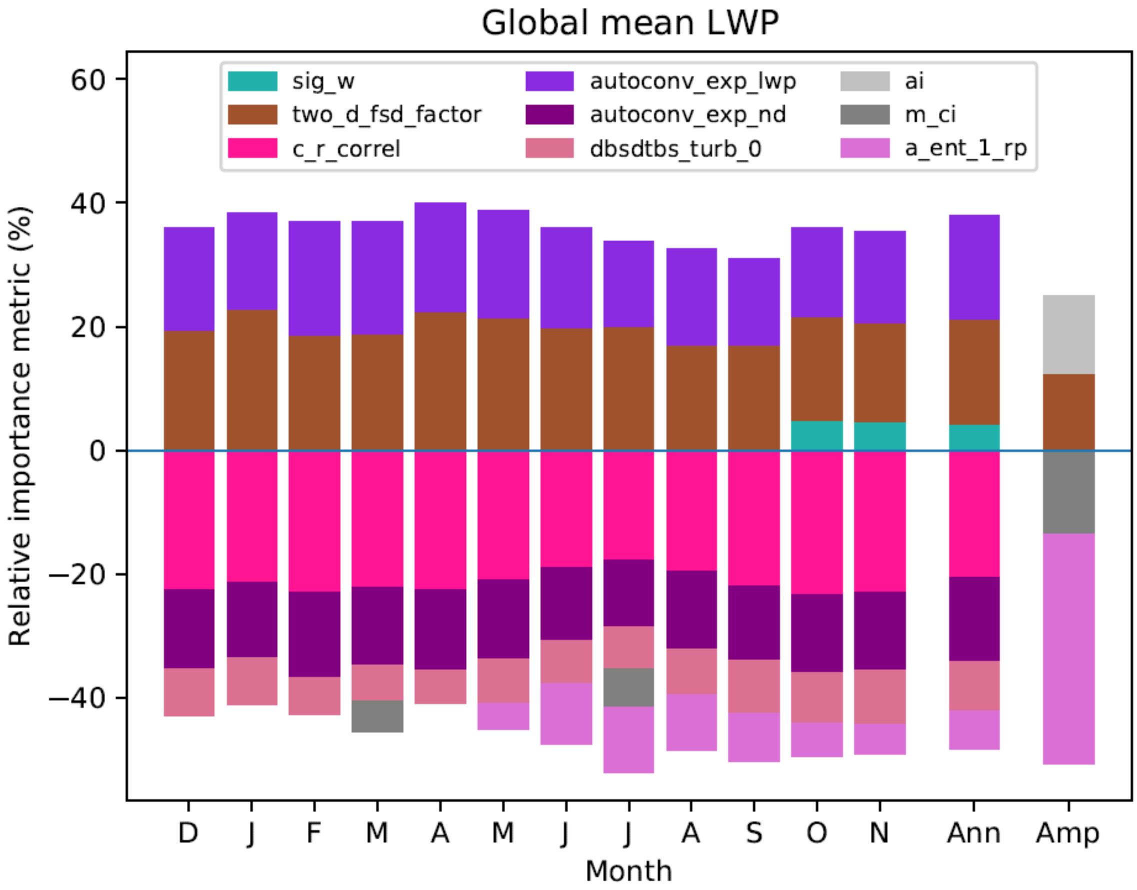

Fig. S19: Relative importance of model parameters as causes of uncertainty in global mean LWP. Figure features are identical to Fig. S15.

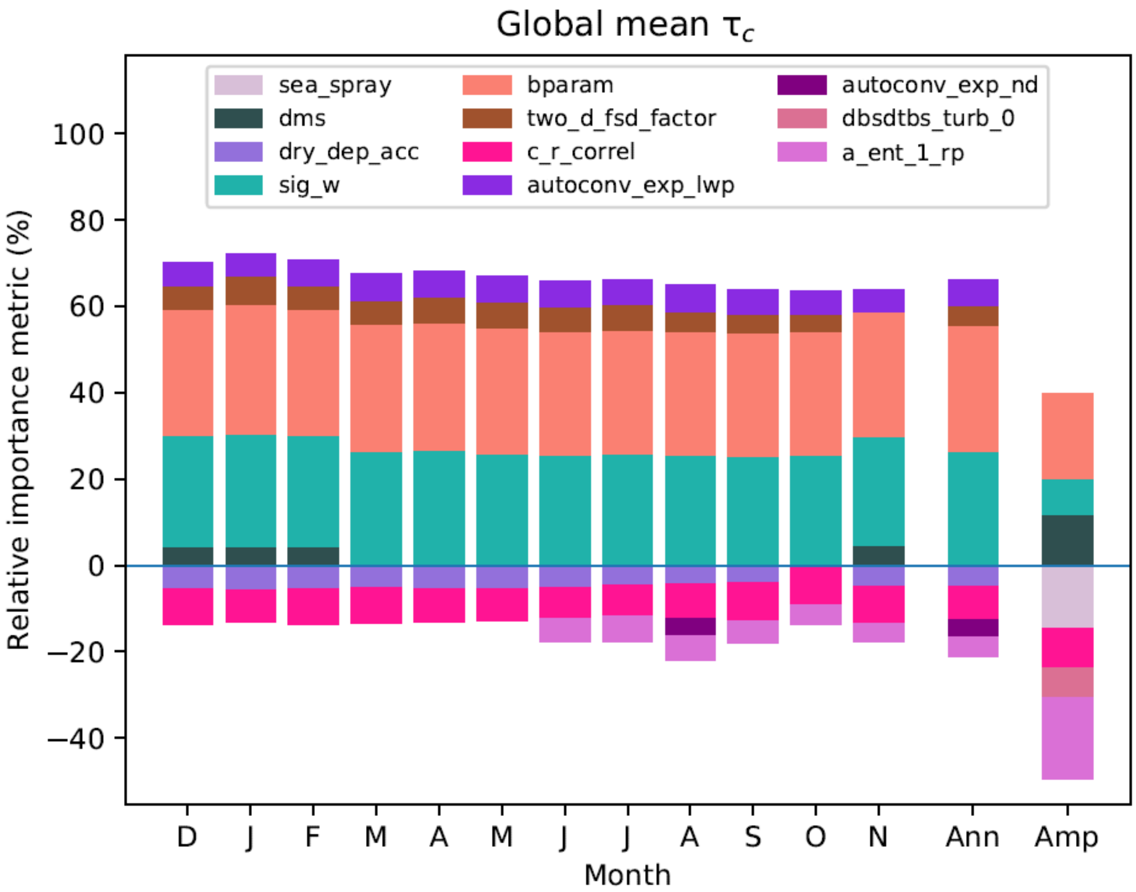

125

Fig. S20: Relative importance of model parameters as causes of uncertainty in global mean τ_c. Figure features are identical to Fig. S15.

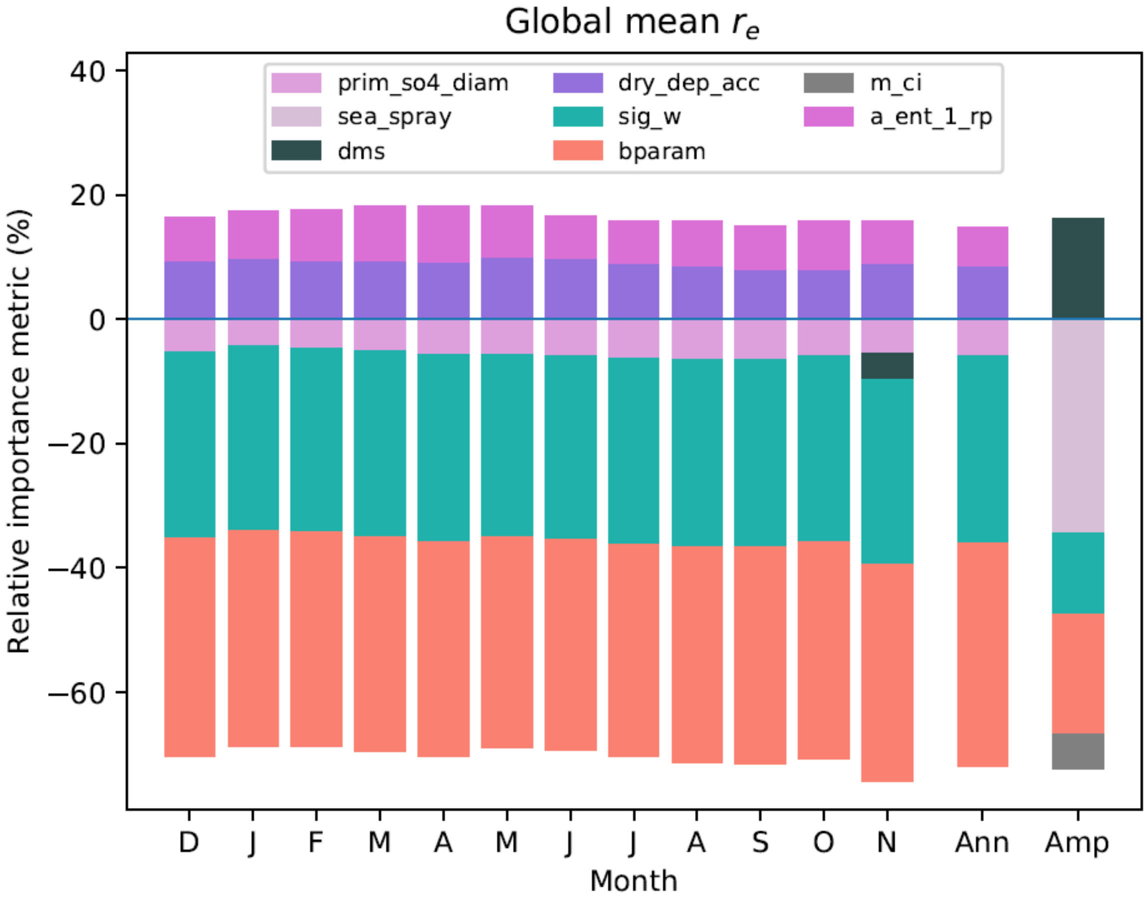

130 **Fig. S21: Relative importance of model parameters as causes of uncertainty in global mean r_e. Figure features are identical to Fig. S15.**

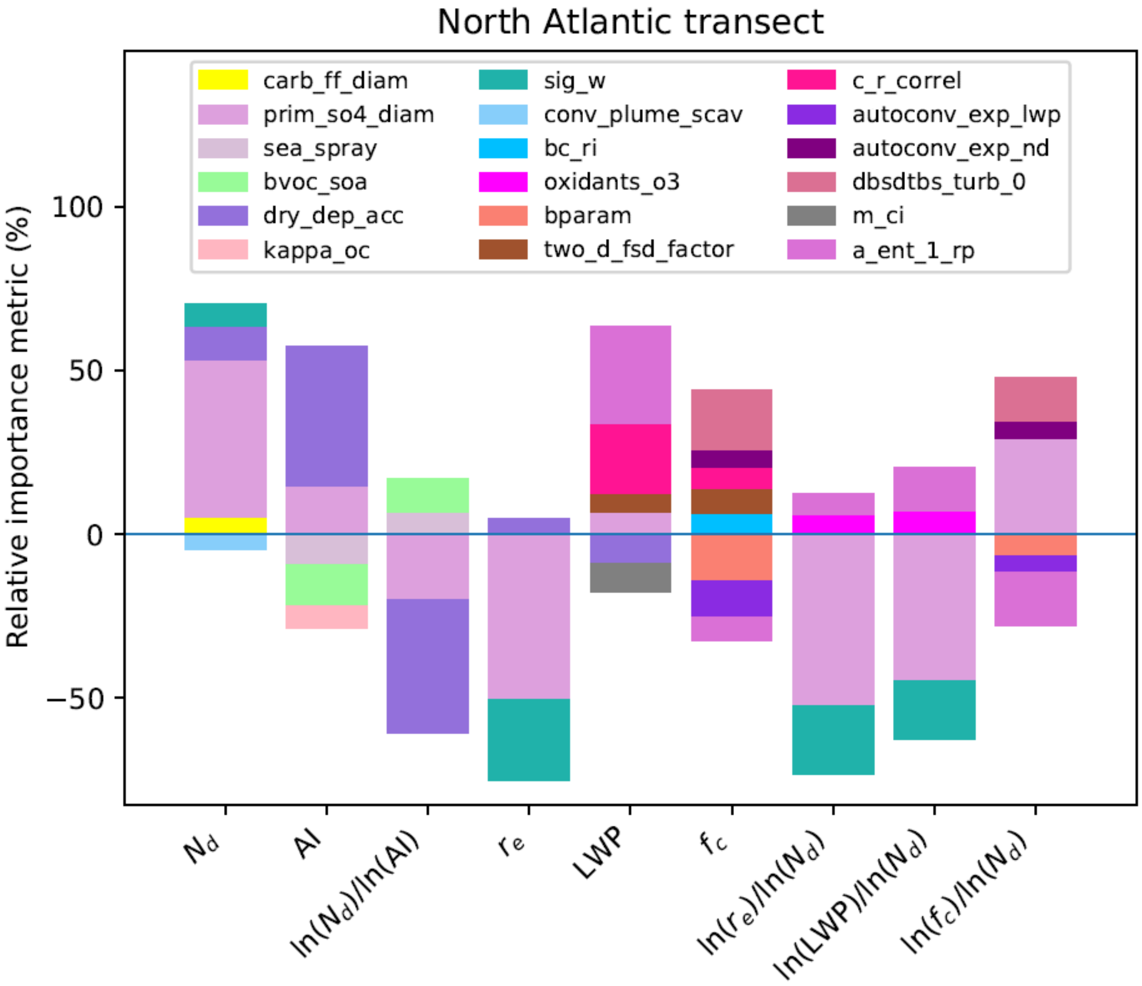

Fig. S22: Relative importance of model parameters as causes of uncertainty in North Atlantic transect constraint variables. Figure features are identical to Fig. S15.

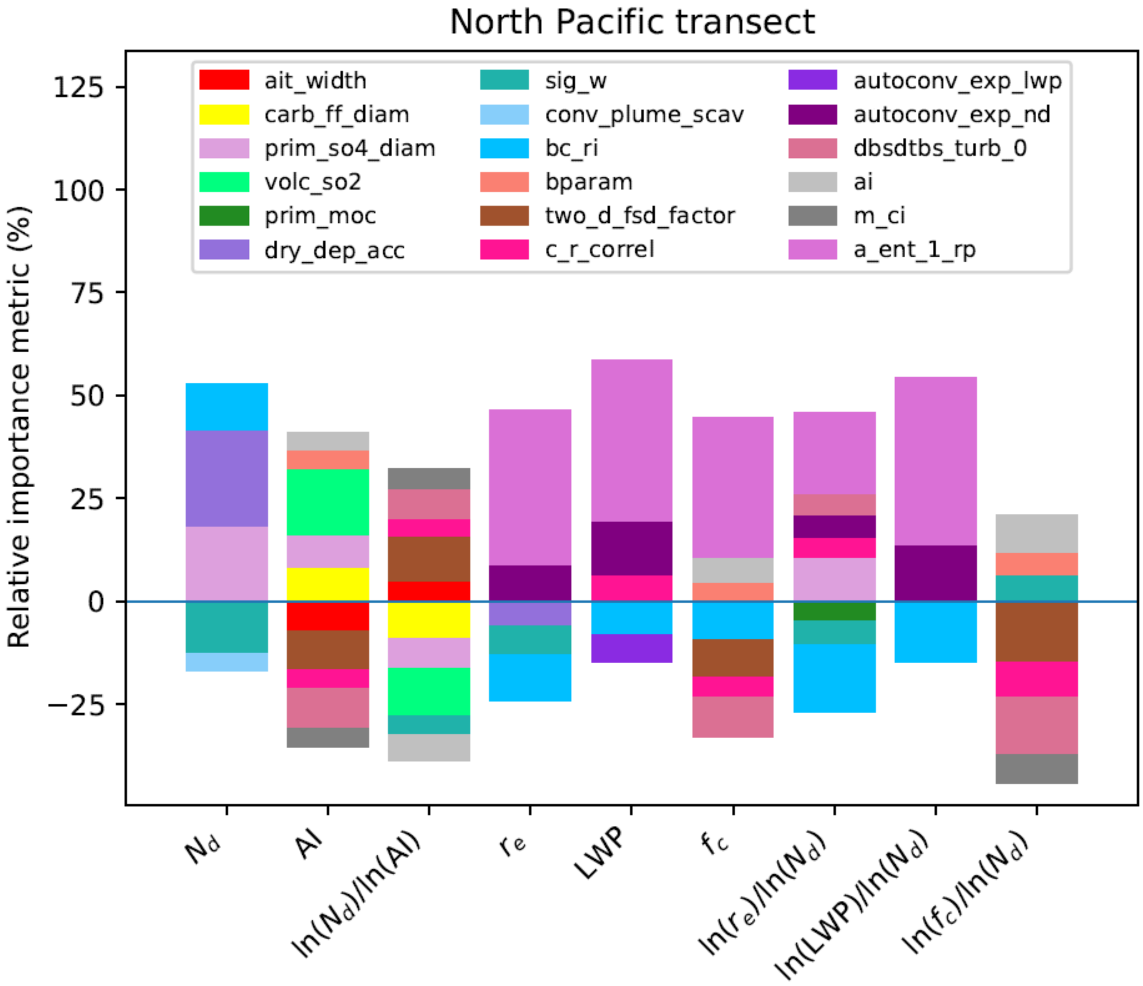

Fig. S23: Relative importance of model parameters as causes of uncertainty in North Pacific transect constraint variables. Figure features are identical to Fig. S15.

140

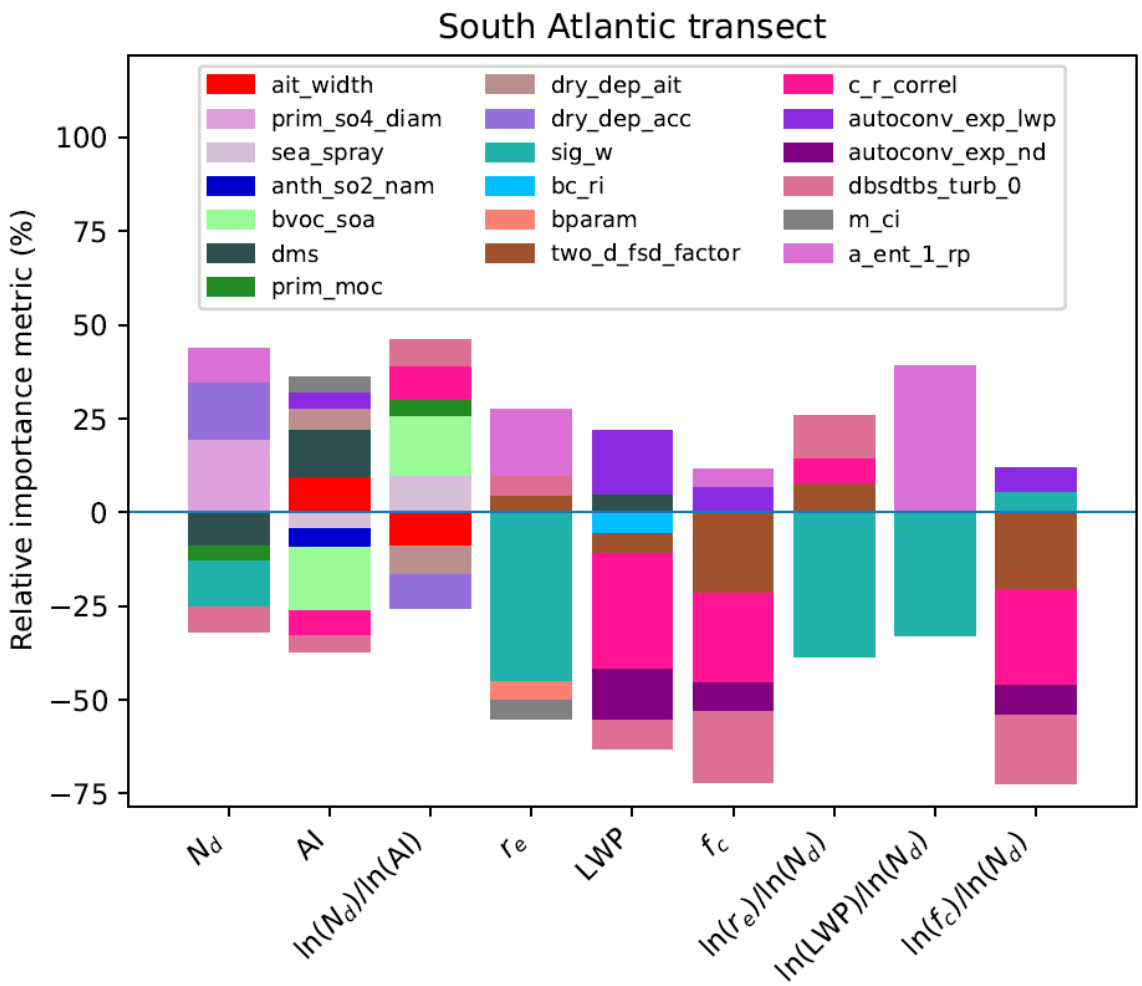

Fig. S24: Relative importance of model parameters as causes of uncertainty in South Atlantic transect constraint variables. Figure features are identical to Fig. S15.

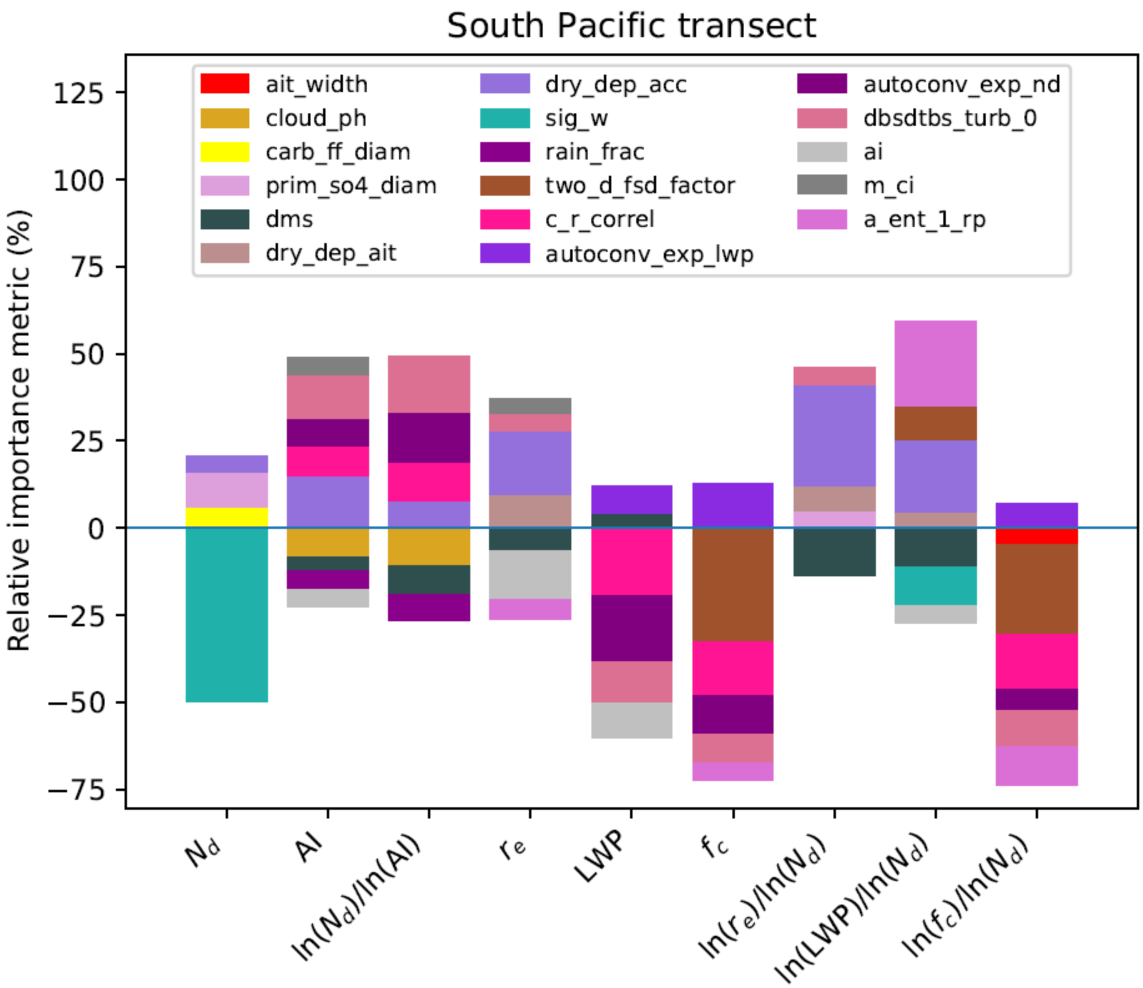

145 **Fig. S25: Relative importance of model parameters as causes of uncertainty in South Pacific transect constraint variables. Figure features are identical to Fig. S15.**

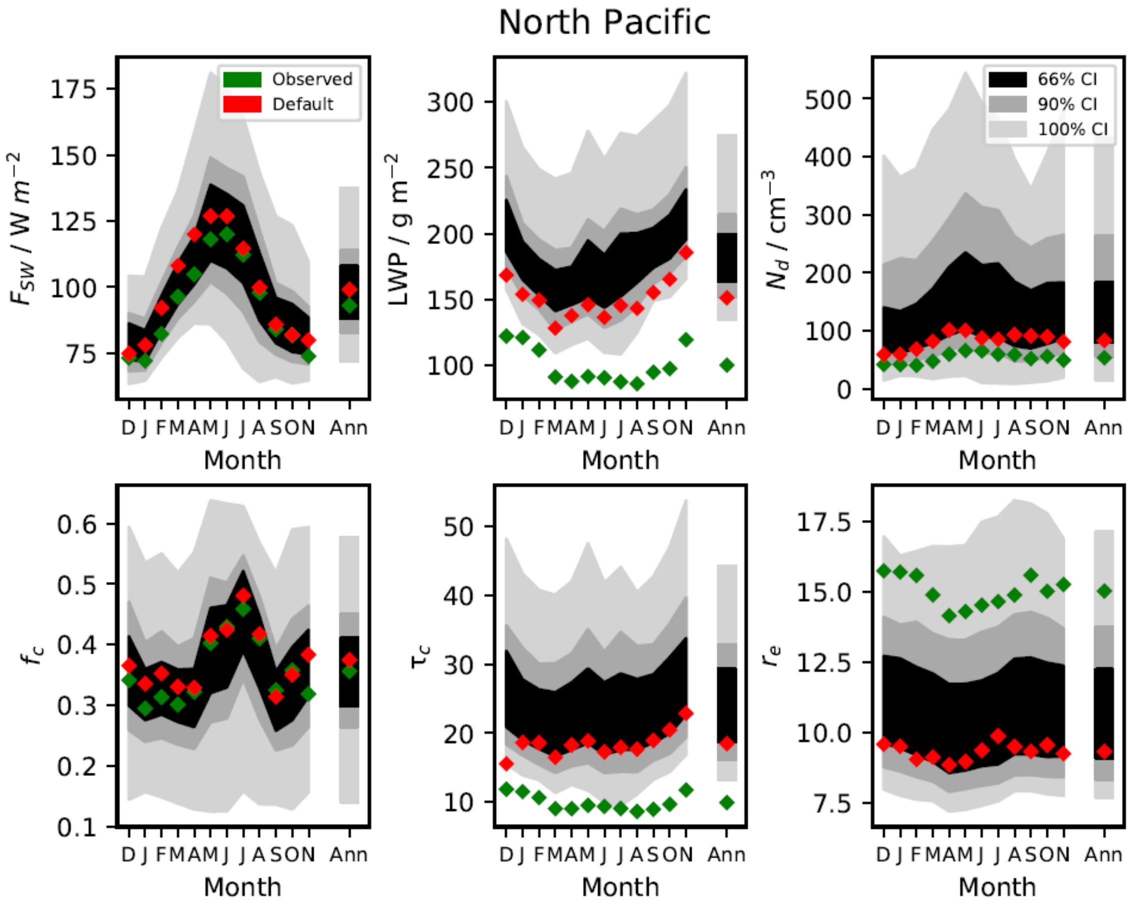

150 **Fig. S26: Probability distributions of North Pacific regional mean output from our sample of model variants, satellite-derived measurements and the default UKESM1-A model, for individual months spanning December 2016 to November 2017 and the annual mean.**

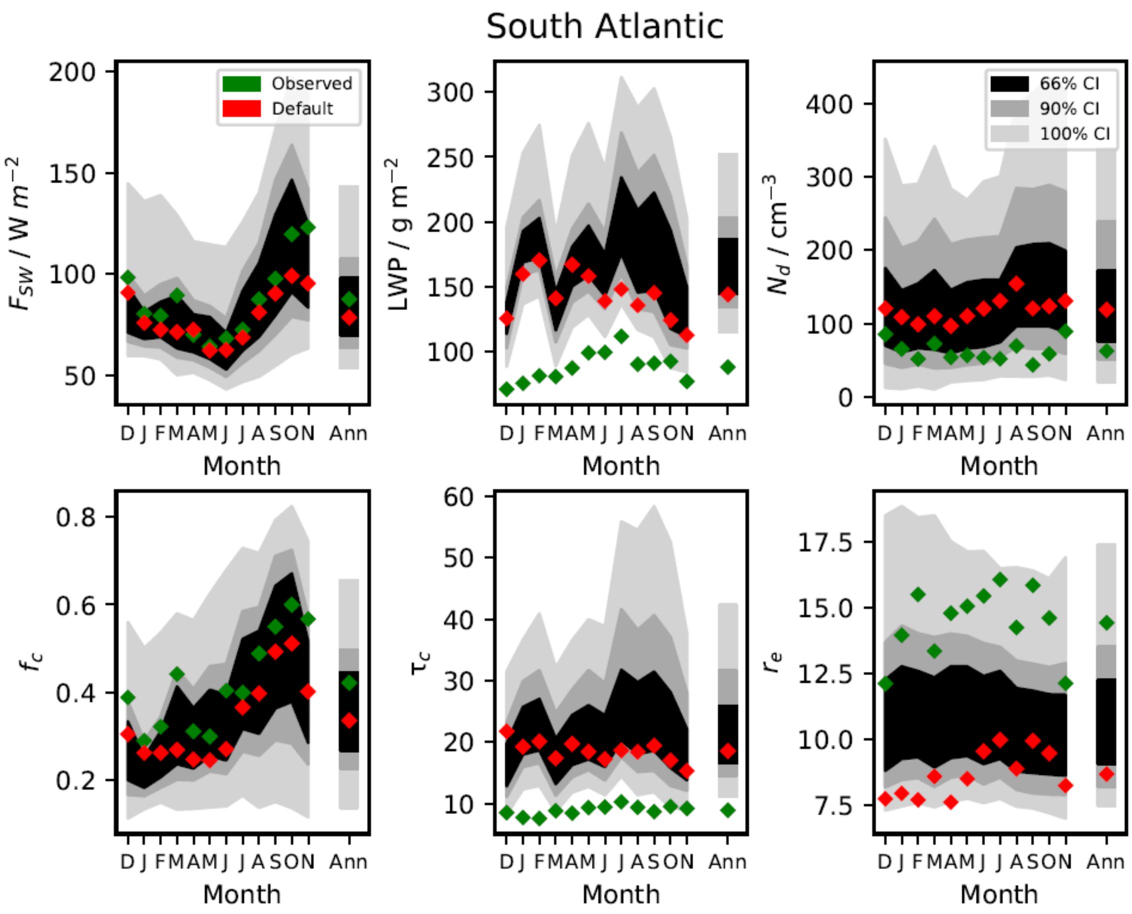

155 **Fig. S27: Probability distributions of South Atlantic regional mean output from our sample of model variants, satellite-derived measurements and the default UKESM1-A model, for individual months spanning December 2016 to November 2017 and the annual mean.**

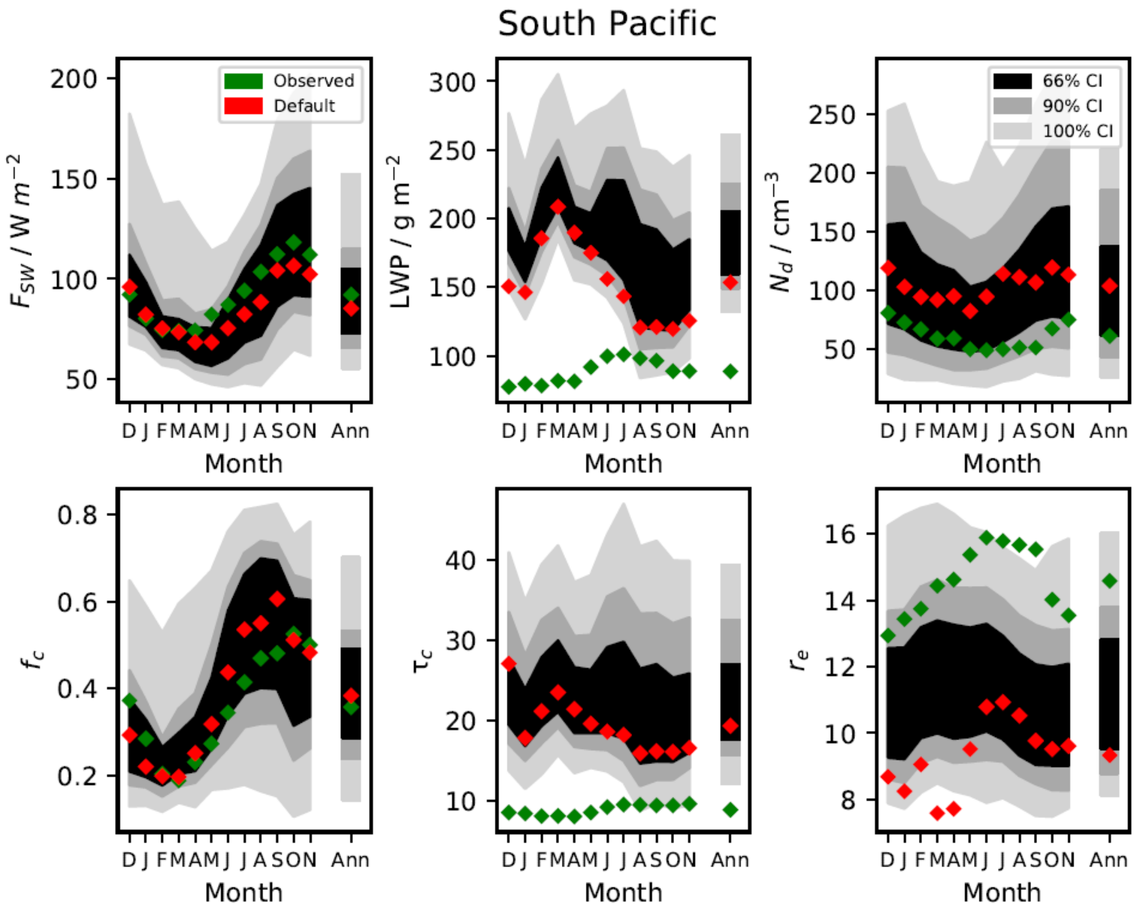

160 **Fig. S28: Probability distributions of South Pacific regional mean output from our sample of model variants, satellite-derived measurements and the default UKESM1-A model, for individual months spanning December 2016 to November 2017 and the annual mean.**

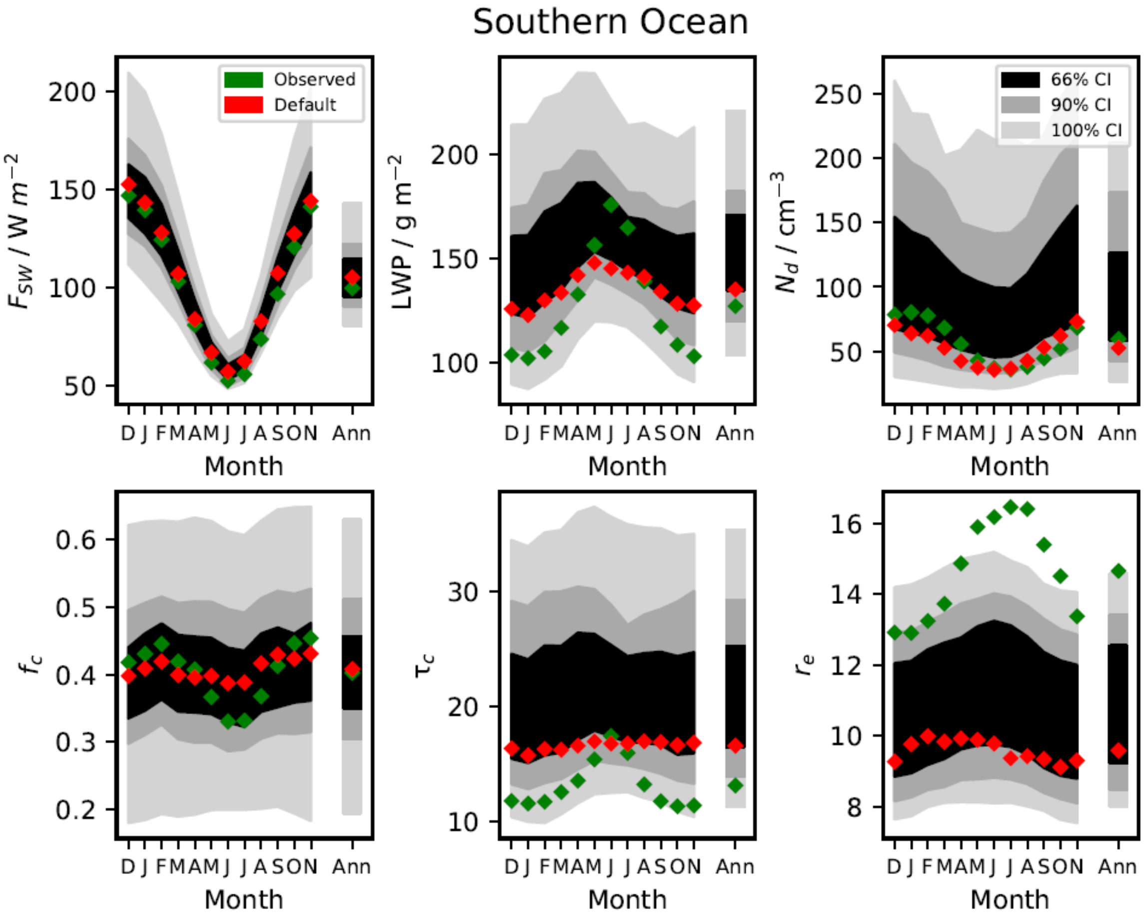

165 **Fig. S29: Probability distributions of Southern Ocean regional mean output from our sample of model variants, satellite-derived measurements and the default UKESM1-A model, for individual months spanning December 2016 to November 2017 and the annual mean.**

Table S1. Parameters perturbed in our PPE, the ranges they were perturbed over and default values as prescribed in the release version of the model. For parameters described as “scale factors”, we perturbed values by scaling the default process parameter value up or down over the indicated range. All other parameters are specific values within the corresponding process parametrizations.

Parameter	Minimum	Maximum	Default	Parameter Description
bl_nuc	0.1	10	1	Boundary layer nucleation rate scale factor
ait_width	1.2	1.8	1.59	Modal width of Aitken modes (nm)
cloud_ph	1e-7	2.51e-5	1e-5	Cloud droplet pH
carb_ff_diam	30	90	60	Emission diameter of carbonaceous aerosol from fossil fuel sources (nm)
carb_bb_diam	90	300	110	Emission diameter of carbonaceous aerosol from biomass burning sources (nm)
carb_res_diam	90	500	150	Emission diameter of carbonaceous aerosol from residential sources (nm)
prim_so4_diam	3	100	150	Emission diameter of 50% of new sub-grid sulfate particles (nm). Remaining 50% emitted into the larger coarse mode (nm)
sea_spray	0.25	4	1	Sea spray emission flux scale factor
anth_so$_2$	0.6	1.5	1	Anthropogenic SO2 emission flux scale factors. Applied independently to European, North American, Chinese, Asian regions and the rest of the world
volc_so2	0.71	2.38	1	Volcanic SO$_2$ emission flux scale factor
bvoc_soa	0.32	3.68	1	Biogenic monoterpene production rate of secondary organic aerosol scale factor
dms	0.33	3	1	Dimethyl-sulfide emission flux scale factor
prim_moc	0.4	6	1	Primary marine organic carbon emission flux scale factor
dry_dep_ait	0.5	2	1	Dry deposition velocity of Aitken mode aerosol
dry_dep_acc	0.1	10	1	Dry deposition velocity of accumulation mode aerosol
dry_dep_so2	0.2	5	1	Dry deposition velocity of SO$_2$
kappa_oc	0.2	0.65	0.65	Hygroscopicity parameter κ for organic aerosol – affects wet diameter and clear-sky radiative flux
sig_w	0.25	1.75	1	Standard deviation of shallow-cloud updraft velocity scale factor
rain_frac	0.3	0.7	0.3	Fraction of cloud covered area where rain forms
cloud_ice_thresh	0.1	0.5	N/A	Threshold of cloud ice water fraction for scavenging
conv_plume_scav	0	0.5	0.5	Scavenging efficieny (as a fraction of total aerosol removed) of Aitken mode aerosol in convective clouds
bc_ri	0.2	0.8	0.565	Imaginary part of the black carbon refractive index

oxidant_oh	0.7	1.3	1	Offline oxidant OH concentration scale factor
oxidants_o3	0.7	1.3	1	Offline oxidant O_3 concentration scale factor
bparam	-0.15	-0.13	-0.14	Coefficient of the spectral shape parameter β for effective radius
two_d_fsd_factor	1	2	1.4	Scale factor for the 2D relationship between cloud condensate variance, cloud cover and convection. Cotrols sub-grid cloud heterogeneity
c_r_correl	0	1	0.9	Cloud and rain sub-grid horizontal spatial colocation
autoconv_exp_lwp	2.15	3.31	2.47	Exponent of liquid water path in the power law for initiating autoconversion
autoconv_exp_nd	-3	-1	-1.79	Exponent of cloud droplet concentration (N_d) in the power law for initiating autoconversion
dbsdtbd_turb_0	0	1e-3	1.5e-4	Cloud erosion rate (s^{-1})
ai	0	5e-2	2.57e-2	Scaling coefficient for the dependence of ice mass on diameter
m_ci	0	3	1	Ice fallspeed scale factor
a_ent_1_rp	0	0.5	0.23	Cloud top entrainment rate scale factor

Table S2. Regions of persistent stratocumulus cloud used to calculate regional mean constraint variables.

Region	Latitude range	Longitude range
North Atlantic	34.4^o to 54.4^o N	329.1^o to 347.8^o E
North Pacific	14.4^o to 48.1^o N	197.8^o to 231.6^o E
South Atlantic	30.6^o to 10.6^o S	347.8^o to 2.8^o E
South Pacific	30.6^o to 15.6^o S	254.1^o to 284.1^o E
Southern Ocean	30.6^o to 50.6^o S	0^o to 360^o E

Table S3. Transects from stratocumulus- to cumulus-dominated regions.

Region	Start position	End position
North Atlantic	54.4º N, 336.6º E	45.6º N, 330.9º E
North Pacific	30.6º N, 229.7º E	19.4º N, 227.8º E
South Atlantic	11.9º S, 357.2º E	11.9º S, 345.9º E
South Pacific	20.6º S, 282.2º E	15.6º S, 269.1º E

Table S4. Effect of varying the number of model variants retained at each stage of constraint. We show the number of constraint variables needed to optimally constrain ΔF_{aer} and the 90% CI in each case.

Number of model variants retained	Number of measurements used	Lower, negative ΔF_{aer} bound	Upper ΔF_{aer} bound
1000	27	-1.15	-0.07
2000	31	-1.23	-0.10
5000	13	-1.26	-0.13
10000	29	-1.30	-0.13
20000	15	-1.33	-0.13